

Article

Numerical Study on the Effects of the Multiple Porous Medium Breakwaters on the Propagation of the Solitary Wave

Kui Zhu ¹, Runxiang Jiang ¹, Zhaolong Sun ¹, Hao Qin ², Zeqi Cheng ², Yang Wang ^{3,*} and Enjin Zhao ² 

¹ College of Electrical Engineering, Naval University of Engineering, Wuhan 430033, China

² College of Marine Science and Technology, China University of Geosciences, Wuhan 430074, China

³ Haikou Marine Geological Survey Center, China Geological Survey, Haikou 570100, China

* Correspondence: wangyang01@mail.cgs.gov.cn

Abstract: Submerged breakwater, as an important marine engineering structure, can effectively absorb wave energy and is widely used in marine engineering protection. As a new type of breakwater, porous medium breakwater has a certain influence on wave propagation. However, the influence of multiple porous medium submerged breakwaters on extreme waves remains to be studied. In the study, considering effects of extreme waves generated by hurricanes or tsunamis, the influence of the solitary wave on the multiple semi-circle porous medium breakwater is systematically investigated. According to the computational fluid dynamics theory, a numerical tank is established, in which the porous medium module is coupled. The computational capability of this model is verified first. Then, depending on the model, a series of cases are carried out to study the effects of different porous medium breakwaters on the propagation of the solitary wave. The results show that when the porosity is 0.8, the force on the submerged breakwaters is the smallest, and the water level and the velocity decrease seriously. With the increase in the diameter of the submerged breakwater, the wave profile gradually becomes flat. The higher the wave height, the more serious the wave deformation after passing through the submerged breakwater.



Citation: Zhu, K.; Jiang, R.; Sun, Z.; Qin, H.; Cheng, Z.; Wang, Y.; Zhao, E. Numerical Study on the Effects of the Multiple Porous Medium

Breakwaters on the Propagation of the Solitary Wave. *J. Mar. Sci. Eng.* **2023**, *11*, 565. <https://doi.org/10.3390/jmse11030565>

Academic Editors: M. Dolores Esteban, José-Santos López-Gutiérrez, Vicente Negro and M. Graça Neves

Received: 20 January 2023

Revised: 19 February 2023

Accepted: 23 February 2023

Published: 7 March 2023



Copyright: © 2023 by the authors. Licensee MDPI, Basel, Switzerland. This article is an open access article distributed under the terms and conditions of the Creative Commons Attribution (CC BY) license (<https://creativecommons.org/licenses/by/4.0/>).

Keywords: hydrodynamic load; porous medium; flow field; submerged breakwater

1. Introduction

Waves are an important dynamic factor in the ocean. In order to weaken the influence of the wave on the coastal structures, a breakwater is constructed, which is a hydraulic structure to block the wave propagation and keep the water surface stable. The interaction between the wave and the breakwater has received much attention in coastal engineering and it is necessary to study the hydrodynamic characteristics around the breakwater to ensure its safe and application.

Therefore, various breakwaters are developed and investigated [1–3]. Osman et al. numerically investigated soliton wave solutions, solitary wave solutions and so on. They used a range of methods including generalized Kudryashov and Chebyshev series to obtain exact travelling wave solutions of nonlinear evolution equations [4–6]. Han and Dong investigated the interaction between solitary waves and submerged breakwaters based on smoothed particle hydrodynamics, which showed that the potential energy is transmitted more easily through a submerged breakwater than kinetic energy [7]. Nassiraei et al. investigate the long wave (tsunami) forces on caisson breakwaters using numerical modeling. Verifications of the simulation results using experimental data, analytical formulas and empirical formulas show that a numerical model is capable of modeling the aforesaid problem with enough accuracy [8]. Mahmoudof and Hajivalie numerically studied the hydraulic response of smooth submerged breakwaters (SMB) to irregular waves and proposed a comprehensive parameter to describe the responses, transmission, and reflection of SMB [9]. Zhao et al. investigated the wave interaction with a fluid-filled-membrane-submerged

breakwater. A modified ghost-cell immersed boundary method was adopted. The results showed that, in lower excess internal pressure, the wave reflection, vortex shedding and energy dissipation were significant [10]. Bautista et al. studied the interaction between long water waves and two fixed submerged breakwaters of wavy surfaces, which showed that the largest values of the reflection coefficient occur for large values of the number of the undulations on the wavy surfaces [11]. Chen et al. investigated wave interaction with a twin floating breakwater through an introduced a mooring line computation δ -SPH model, which indicated that the twin floating breakwater is superior to the single pontoon floating breakwater on wave-attenuation performances [12]. Liang et al. investigated the interaction between a new box-type breakwater and the wave which showed that a larger deck width for the proposed breakwater was more conducive to dissipating the energy of longer period waves [13]. Magdalena et al. used three-layer depth-integrated equations to calculate wave amplitude reduction in a domain with n submerged porous media blocks. When one of the two layers has a greater friction coefficient, increasing its thickness will produce a greater wave attenuation [14]. Aristodemo and Filianoti performed laboratory experimental and δ -LES-SPH simulations to analyze solitary wave-induced forces at submerged rigid breakwaters. It was found that, by increasing the relative height of the breakwaters, the wave loads tended to grow, particularly for the horizontal ones [15]. Liang et al. studied the wave transmission over double submerged breakwaters using non-hydrostatic wave model SWASH. It was found that dissipation of super harmonic wave components is more obvious than that of lower harmonic wave components [16]. Lyu et al. developed an iterative multipole solution for water wave interaction with a submerged, partially perforated semi-circular breakwater based on the linear potential theory. The results showed that enlarging porosity will significantly decrease wave reflection and horizontal wave force, but has little effect on vertical wave force [17]. Liu and Wang studied the box-type floating breakwaters, extensively using the SPH. The results showed that the larger and lighter the breakwaters, the better the performance is [18]. Metallinos et al. simulated the regular and irregular wave propagation over the submerged porous breakwaters using an extended Boussinesq-type model, which showed that the porous medium break can effectively weaken wave propagation [19]. Li and Zhang investigated the effects of three-dimensional interactions of obliquely incident waves and breakwaters on wave potential energy reduction based on the energy transmission coefficient. The transmitted wave energy was reduced more significantly as the incident wave steepness increases or the submergence depth decreases, since more agitation occurs around the breakwater [20].

In addition to the investigation between the wave and the breakwater, the protection of the breakwater to the different coastal structures was also studied. Xue et al. studied the influence of the breakwater composed of three identical semicircular shells and a rectangular base on the wave loads on the coastal bridges. The results demonstrated an increased effectiveness of this breakwater to dissipate wave energy [21]. Sun et al. numerically investigated the effects of the submerged porous breakwater, which showed that the breakwater is effective in reducing the hydrodynamic loads applied to the coastal bridge decks [22]. Patil and Karmakar investigated the wave interactions with the submerged rubble mound breakwater (SRMB) and the submerged floating tunnel (SFT) using multi-domain boundary element method (MDBEM). Due to the SFT, the SFT's safety is improved [23]. He et al. established a mathematical model to solve the wave diffraction and radiation problem of floating piers with a submerged annular ripple breakwater. It was found that the wave excitation force and hydrodynamic coefficient of the floating pier change periodically with the increase in the distance from the breakwater [24]. Zhao et al. investigated the effects of the different porous medium breakwaters on the propagation and run-up of the solitary wave. With the increase in the wave height, the force difference attenuation coefficient on the breakwater decreases [25]. Guo et al. developed an analytical model for a submerged breakwater over variable bottom topography based on linear wave theory. It was found that the full-wave reflection is drastically reduced and the wave energy is dissipated [26].

Koley et al. investigated the performance of a submerged flexible porous membrane which is floating over a porous breakwater. The results demonstrated that the resonating behavior diminishes with the introduction of structural porosity in the membrane wave barrier [27]. Koraim et al. experimentally studied the hydrodynamic efficiency of a porous seawall under the regular wave, in front of which is a submerged breakwater. The submerged breakwater decreases the run-up on the seawall [28].

As a new type of marine protection structure, porous medium breakwaters have a certain influence on wave propagation. However, the influence of multiple porous medium submerged breakwater on extreme waves remains to be studied. Based on the previous study, this paper continues to improve the submerged theory and compares the different influence under different waves, which provides technical support for marine engineering construction. The rest of this paper is organized as follows. Section 2 introduces the numerical model. The verification of the model is conducted in Section 3. Section 4 discusses the effects of the multiple porous medium breakwater on the propagation of the solitary wave. Section 5 provides some concluding remarks.

2. Numerical Model

OpenFOAM (Open Field Operation and Manipulation), as an open source computational fluid dynamics software, is more and more widely used in the field of coastal engineering. The governing equations of incompressible fluid in numerical simulation include mass conservation equation and momentum equation, as follows:

$$\nabla \cdot \vec{u} = 0 \tag{1}$$

$$\frac{\partial \rho \vec{u}}{\partial t} + \nabla \rho \vec{u} \vec{u}^T = -\nabla p_r + \mathbf{g}(\mathbf{x} - \mathbf{x}_r) \nabla \rho + \mu_t \nabla \vec{u} \tag{2}$$

where ρ is the fluid density, u is velocity vector in Cartesian coordinate system, t is the time, $\nabla = (\partial/\partial x, \partial/\partial y, \partial/\partial z)$ is the differential operator; p_r is the relative pressure which is expressed as $p_r = p - \rho g x$; p is the total pressure; g is the acceleration of the gravity; $\mathbf{x} = (x, y, z)$ is the vector of spatial coordinates in Cartesian coordinate system; \mathbf{x}_r is the reference position coordinate; and μ_t is the dynamic viscosity.

In the porous medium structure, the velocity through the structure decreases, and the velocity is defined as the transfer velocity, which is related to the velocity in the porous medium object with the porosity (n), as follows:

$$\vec{u} = n \vec{u}_p \tag{3}$$

where \vec{u}_p is the velocity in the porous medium; Jensen (2014) [29] improved the momentum equation in the permeable layer; The continuity equation is the same as in the previous section, while the momentum equation is modified as follows:

$$(1 + C_m) \frac{1}{n} \frac{\partial \rho \vec{u}}{\partial t} + \frac{1}{n^2} \nabla \rho \vec{u} \vec{u}^T = -\nabla p_r + \mathbf{g}(\mathbf{x} - \mathbf{x}_r) \nabla \rho + \frac{1}{n} \mu_t \nabla \vec{u} - \mathbf{F}_p \tag{4}$$

where the additional quality coefficient C_m is as follows:

$$C_m = \gamma_p \frac{1 - n}{n} \tag{5}$$

where γ_p is the closure coefficient which is 0.34.

The resistance formula is as follows:

$$\mathbf{F}_p / \rho = a \vec{u} + b \vec{u} \|\vec{u}\|_2 \tag{6}$$

where a and b are the resistance coefficients. In the formula proposed by Van Gent (1995) [30], the resistance coefficients a and b are calculated as follows:

$$a = \alpha \frac{(1 - n)^2}{n^3} \frac{v}{d_{50}^2} \tag{7}$$

$$b = \beta \left(1 + \frac{7.5}{KC}\right) \frac{1 - n}{n^3} \frac{1}{d_{50}^2} \tag{8}$$

where v is the kinematic viscosity; d_{50} is the median particle diameter of the granular material; and KC is the Keulegan-Carpenter number.

The finite volume method is adopted in the numerical solution, in which the time domain term is discretized by Euler implicit scheme, the convection term is discretized by restricted linear scheme, the diffusion term is discretized by linear scheme, and the source term and the wave-absorbing term are discretized explicitly. The numerical calculation method adopts PIMPLE algorithm, that is, a combination of the SIMPLE algorithm and the PISO algorithm. The basic idea of PIMPLE is to solve each time step with a simple steady-state algorithm (that is, to see each time step as a steady-state flow), and the step of the time step is completed by the PISO algorithm. The PIMPLE algorithm treats each time step as a steady-state flow (using Asunchi to solve the situation of large changes in two adjacent time periods), and when the steady-state solver is solved to a certain extent, the standard PISO is used as the final step of the solution. In this paper, the inlet, outlet, and bottom boundary are set as a solid wall with a non-slip boundary, and the top boundary is in direct contact with the air pressure condition. The tangential velocity is given in inflow, and the gradient of velocity components in all directions is 0 in outflow.

The model uses the VOF method to simulate the tracking of the free surface [31]. The equation is as follows:

$$\frac{\partial F}{\partial t} + \frac{1}{n} (\nabla \vec{u} F + \frac{1}{n} \nabla \vec{u}_r F (1 - F)) = 0 \tag{9}$$

where \vec{u}_r is the relative velocity; F is the VOF function where when it is filled with water, F is 1, and when it is filled with air, F is 0. The intermediate value will be located at or near the interface, the linear weighting method is used as follows:

$$\rho = F\rho_1 + (1 - F)\rho_0 \tag{10}$$

$$\mu = F\mu_1 + (1 - F)\mu_0 \tag{11}$$

where subscript 1 and 0 represent the properties of water and air, respectively.

According to the wave theory, the velocity entrance method specifies the distribution of the velocity field on the wave-making boundary at each time step. Its advantage is to strictly abide by the wave theory. If the target wave is just within the selected wave theory range, it will obtain more accurate results. However, there are two problems in this method: First, when the nonlinearity of the target wave is strong, the speed of input and extraction on the boundary in a wave period is not equal, and with the increase in calculation time, it may lead to problems of mass conservation such as wave surface uplift; secondly, the velocity entrance method cannot eliminate the secondary reflection wave. Therefore, when the velocity entrance method is adopted to simulate waves, corresponding correction measures must be taken [32]. Waves2Foam adopts the method of adding relaxation zones at the front and rear ends of the flume, which not only ensures the conservation of mass, but also eliminates the secondary reflection wave. The relaxation zone technology aims at eliminating false reflection in numerical simulation. The technique is based on the weighting between the calculated solution of the velocity field and the indicated field with the target solution. There are two forms of explicit relaxation and implicit relaxation, in

which explicit/implicit refers to time integration [33]. The explicit method of relaxation zone is as follows:

$$\phi = (1 - \omega_R)\phi_t + \omega_R\phi_c \tag{12}$$

where the weighting function is ω_R as follows:

$$\omega_R = 1 - \frac{\exp \sigma^{3.5} - 1}{\exp 1 - 1} \tag{13}$$

where σ is the local coordinate in the relaxation zone.

A solitary wave, as a kind of nonlinear wave, can keep the shape and energy of waves well in long distance propagation. The wavelength tends to infinity, and the whole wave surface is higher than the still water surface. In fact, solitary waves only have one peak higher than the horizontal plane to propagate forward, which describes a moving wave with non-periodic motion [34]. The relative wave height of solitary wave is the most important factor to determine its waveform. In practical applications, solitary waves are often used to simulate extreme waves such as tsunami waves. The solitary wave used in this paper is the second-order solitary wave. The wave surface equation, water point velocity, acceleration, pressure and wave velocity are expressed as follows:

$$\frac{\eta}{h} = \varepsilon \operatorname{sech}^2 q - \frac{3}{4} \varepsilon^2 \operatorname{sech}^2 q \tanh^2 q \tag{14}$$

$$\frac{p}{\rho gh} = \frac{\eta}{h} + 1 - \frac{s}{h} - \frac{3}{4} \varepsilon^2 \operatorname{sech}^2 q \left[\left(\frac{s}{h} \right)^2 - 1 \right] (2 - 3 \operatorname{sech}^2 q) \tag{15}$$

$$\frac{u}{\sqrt{gh}} = \varepsilon \operatorname{sech}^2 q + \varepsilon^2 \operatorname{sech}^2 q \left[\frac{1}{4} - \operatorname{sech}^2 q - \frac{3}{4} \left(\frac{s}{h} \right)^2 (2 - 3 \operatorname{sech}^2 q) \right] \tag{16}$$

$$\frac{w}{\sqrt{gh}} = \varepsilon \sqrt{3\varepsilon} \left(\frac{s}{h} \right) \operatorname{sech}^2 q \tanh q \left\{ 1 - \varepsilon \left[\frac{3}{8} + 2 \operatorname{sech}^2 q + \frac{1}{2} \left(\frac{s}{h} \right)^2 (1 - 3 \operatorname{sech}^2 q) \right] \right\} \tag{17}$$

$$\frac{c}{\sqrt{gh}} = 1 + \frac{1}{2} \varepsilon - \frac{3}{20} \varepsilon^2 \tag{18}$$

$$q = \frac{\sqrt{3\varepsilon}}{2h} \left(1 - \frac{5}{8} \varepsilon \right) (x - ct) \tag{19}$$

where η represents the water level, p represents the pressure, u represents the horizontal velocity, w represents the vertical velocity, a is the wave height of solitary wave, h is the initial water depth; and the intermediate $\varepsilon = a/h$, $s = z + h$. Theoretically, the water body of the solitary wave peak is always above the still water surface and the theoretical wavelength is infinite.

3. Model Verification

This section may be divided by subheadings. It should provide a concise and precise description of the experimental results, their interpretation, as well as the experimental conclusions that can be drawn.

3.1. Solitary Wave

In order to ensure the simulation accuracy of solitary wave, the solitary wave waveform is first verified. The numerical simulation domain adopted in this study is that the length is 500 m and the height is 14 m. The water depth of the solitary wave is 8 m, and the wave height is 2 m. The wave-making boundary is located at $x = 0$ m. The location of the wave sensor monitor is at $x = 10$ m. Through the comparison between the simulation results and the theoretical wave values, as shown in Figure 1, it can be seen that the theoretical value is in good agreement with the numerical simulation results, which indicates that the established numerical flume can accurately generate solitary waves.

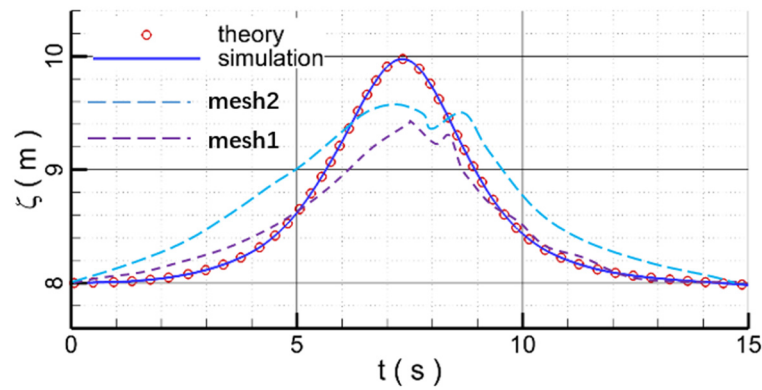


Figure 1. Solitary wave comparison between the theory values and the simulation results.

3.2. Wave Propagation over the Porous Medium Structure

Because this paper mainly discusses the propagation of solitary waves on permeable submerged breakwaters, it is necessary to verify the fluid flow ability of numerical models in permeable structures. The predicted distributions of velocity are compared with the corresponding measured data. The experiment was completed by Wu and Xiao (2013) in a glass flume [35]. The wave flume is 25 m long, 0.5 m wide and 0.6 m deep. The breakwater is composed of uniform glass balls with a diameter of 1.5 cm and a porosity of 0.52, and is installed at the bottom of the flume. The origin of the coordinate system is at the intersection of the bottom and the left side of the breakwater. The length of the simulation area is 8 m. The horizontal resolution of the grid is $dx = 0.004$ m, and the 40 layers are applied in the vertical direction. The distance between the entrance of the simulation domain and the breakwater is 4 m. The still water depth h is 0.106 m, and the incident solitary wave height is 0.0477 m. The Figure 2. shows the velocity and wave surface comparisons.

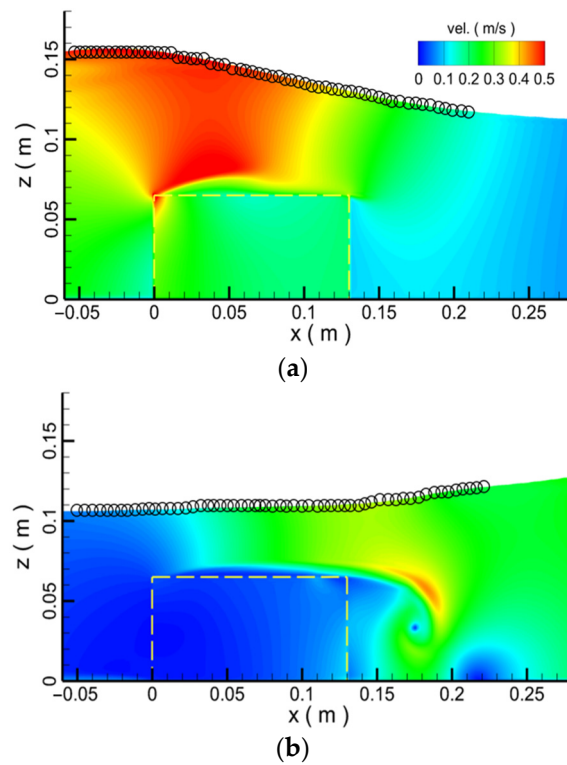


Figure 2. Flow velocity contour; (a) velocity contour; (b) water surface. (the circles represents experimental data).

The distributions of the velocity in horizontal and vertical directions recorded from -0.04 m to 0.2 m are shown in Figure 3. The figure shows that the predicted results are in good agreement with the experiment data. Overall, results clearly support the computational capability of our numerical model for describing a solitary wave propagating over the permeable breakwater.

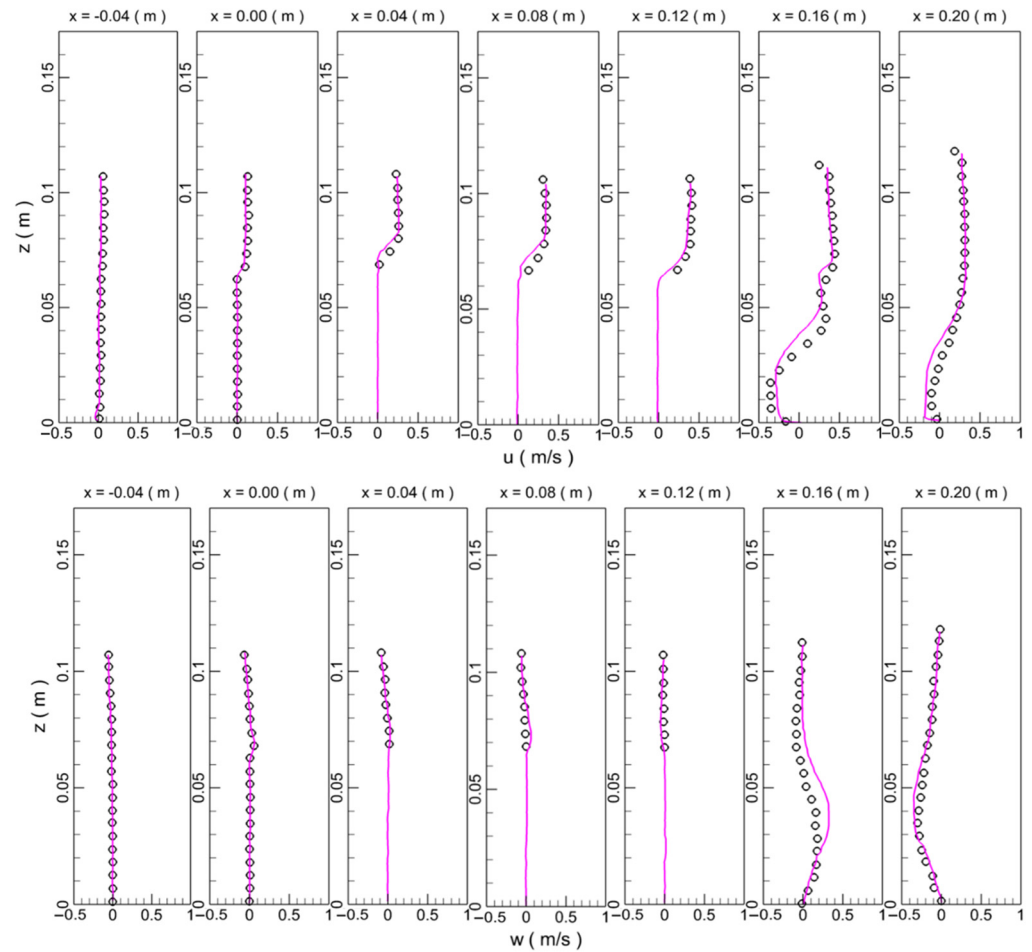


Figure 3. Comparison of velocity distribution between computation and measurement; (u) horizontal velocity; (w) vertical velocity; at $t = 1.65$ s.

4. Results and Discussion

Based on the verified numerical model, this section mainly discusses the influence of multiple porous semi-circular breakwaters on solitary wave propagation. The experimental layout is shown in Figure 4. The whole calculation domain is 500 m long and 16 m high. The diameter of the submerged breakwater is D . The distance between the adjacent submerged breakwaters is s . The static water depth is 8 m. The grid resolution around the submerged breakwater is 0.001 m. The center point of the first submerged breakwater is located at $x = 40$ m. Ten wave sensor monitors and velocity sensors are distributed above the submerged breakwater, at the positions of $x = 10, 20, 30, 40, 50, 60, 70, 80, 90,$ and 100 m. In order to compare and analyze the force efficiently, all the forces are normalized by $\rho g v$.

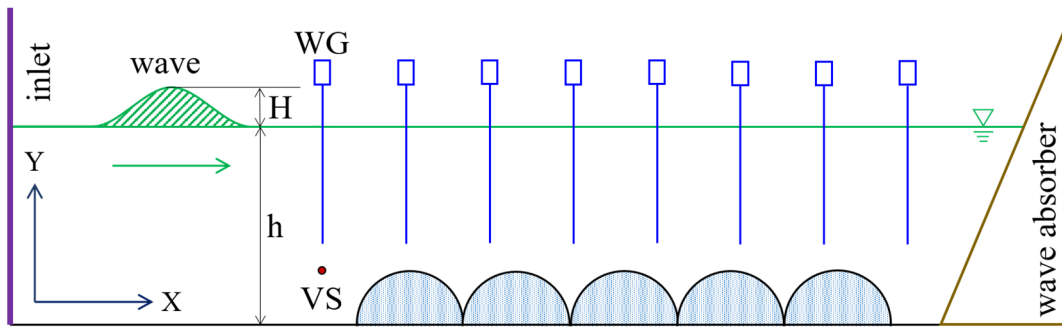


Figure 4. Computational layout for solitary wave passing over the breakwaters.

4.1. Effect of the Porosity

In this section, the influence of the breakwaters with different porosities on the propagation of the solitary wave is analyzed. Seven porosities are selected as 0.0, 0.2, 0.4, 0.5, 0.6, 0.8, and 1.0. Figure 5a shows the velocity contour of solitary waves passing over the multiple porous medium breakwaters. When the solitary wave approaches the submerged breakwater, the water level rises and the velocity increases. When the wave peak propagates to the first submerged breakwater, the velocity around the first submerged breakwater increases. When the wave crest is just above the submerged breakwater, it can be seen that the flow velocity between the water surface and the submerged breakwater are at the maximum, which indicates that the water flux per unit area increases and the overall velocity increases. In addition, the velocity inside the submerged breakwater also increases. Due to the shelter effect of submerged breakwaters, the velocity of flow between submerged breakwaters is low. When the wave peak passes over the submerged breakwater, the velocity in the gap of the submerged breakwater is larger than that in other parts, indicating that the flow in the gap is stronger due to the influence of the submerged breakwater. Figure 5b shows the vorticity contour field of solitary wave passing over the porous breakwaters. When the wave propagates to the submerged breakwater, the vortex begins to appear on the surface of the submerged breakwater due to the barrier of the submerged breakwater. When the wave peak is on the submerged breakwater, the vortex appears above each submerged breakwater, which indicates that the submerged breakwater has a certain blocking effect on the wave. The vortex gradually decreases from the foremost submerged breakwater to the rearmost submerged breakwater. After the wave crest passes over the submerged breakwater, the vortex attached to the submerged breakwater begins to grow and fall off. Due to the influence of the porous submerged breakwater, at the interface between the water body and the submerged breakwater, the vortex is flattened and presents a strip shape, and the tailed vortex presents a circle shape. Figure 6. shows the maximum velocity on the fourth and fifth breakwater at different time.

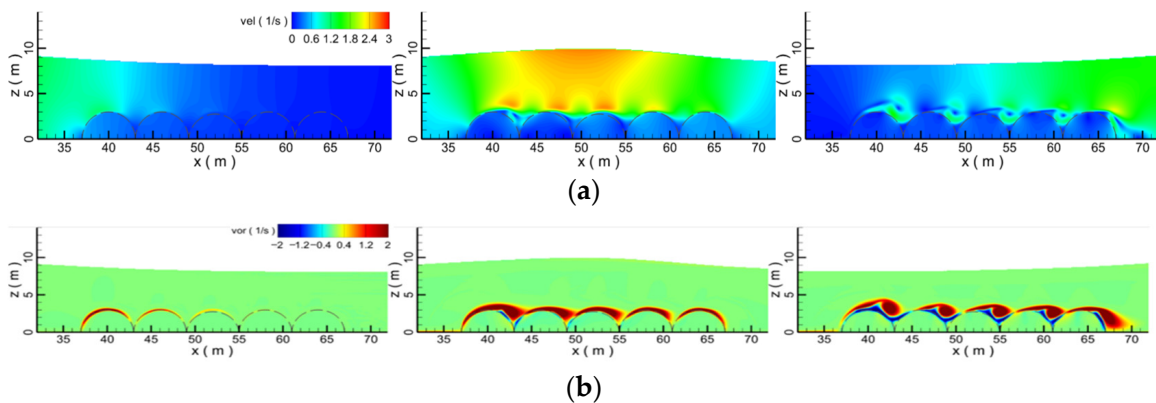


Figure 5. The flow field around the breakwaters at different times; (a) velocity contour; (b) vorticity contour.

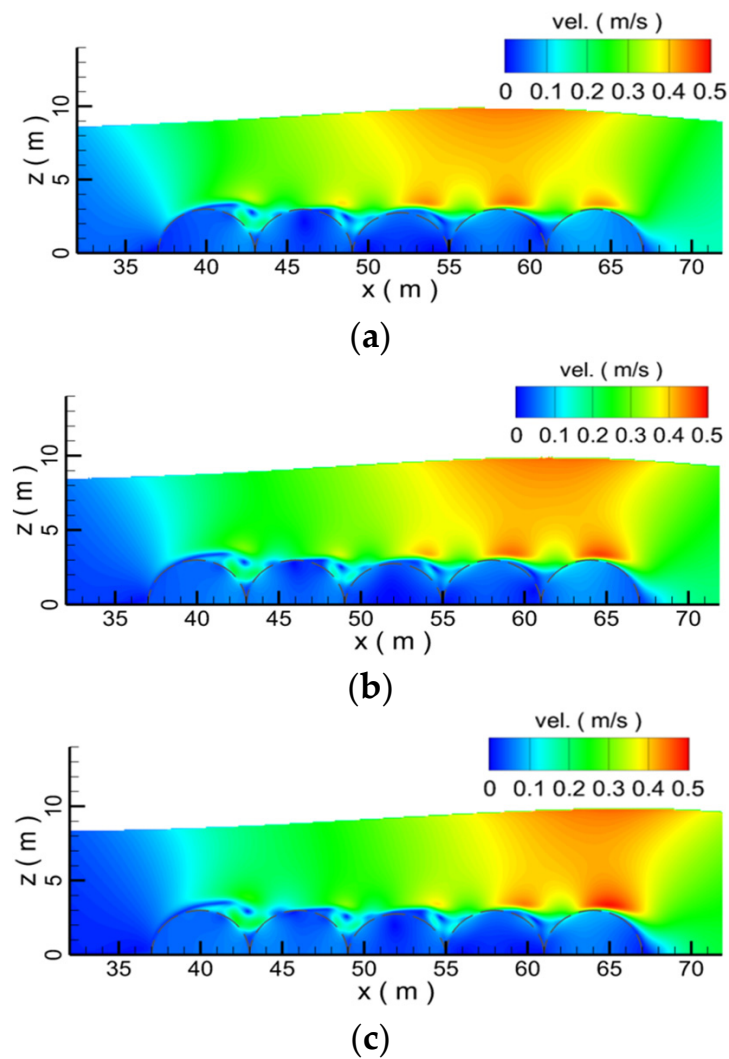


Figure 6. Maximum velocity on the fourth and fifth breakwater; (a) $t = 12.4$ s; (b) $t = 12.8$ s; (c) $t = 13.2$ s.

When the solitary wave passes over the submerged breakwater, Figure 7 shows the velocity contour under different porosities. When the porosity is 0, the submerged breakwater is solid. Since water can not pass through the submerged breakwater, the flow between the submerged breakwater and the water surfaces is the largest. Compared with the velocity above the submerged breakwater with pores, the velocity above the solid breakwater is the highest. With the increase in porosity, the flow passing through the porous submerged breakwater increases, and the velocity between the submerged breakwater and the water surfaces decreases. The velocity in the front submerged breakwater is the smallest, and the velocity in the rear submerged breakwater increases gradually, because the solitary peak has passed over the front breakwater. In addition, the various submerged breakwaters have different influences on the wave. When the porosity is 0.8, the velocity between the first and second submerged breakwaters is about 0.3 m/s, while the velocity in the fourth and fifth pores is 0.6 m/s. When the submerged breakwater does not exist, the velocity distribution of the whole flow field is uniform, and the maximum velocity is 2.0 m/s. In a word, submerged breakwaters with different porosities have different interference effects on the flow field, resulting in the change of velocity distribution in the whole flow field, thus affecting the propagation of solitary waves.

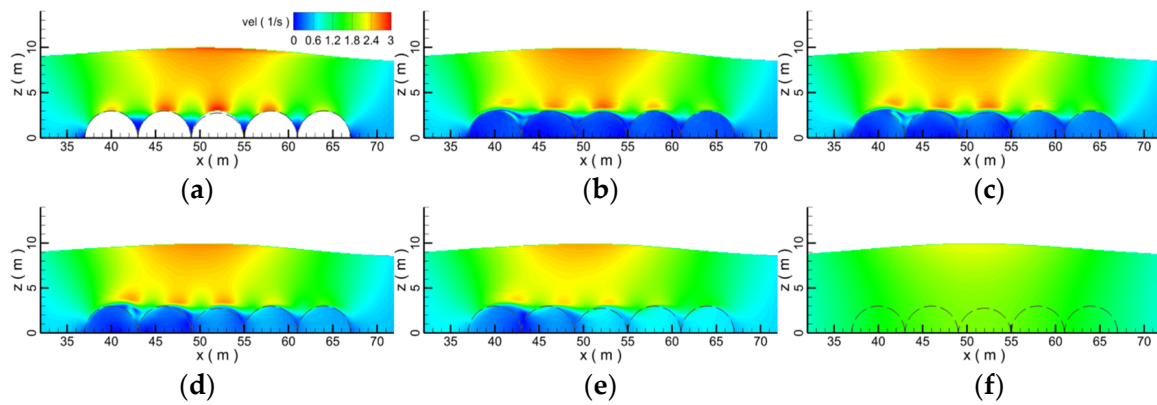


Figure 7. The velocity contour of the wave peak on the breakwaters under different porosities; (a) por = 0.0; (b) por = 0.2; (c) por = 0.4; (d) por = 0.6; (e) por = 0.8; (f) por = 1.0.

Figure 8 shows the vorticity contour around submerged breakwaters with different porosities. It can be seen that when the porosity is 0, the submerged breakwater is solid. The vorticity above the submerged breakwater is small. With the increase in porosity, the vorticity above the submerged breakwater increases. When there are pores in the submerged breakwater, the flow can pass through the submerged breakwater in the pores, and the flow interaction between the inside and outside the submerged breakwater leads to the increase in the flow intensity in the flow field. At the surface of the submerged breakwater, there are also some small vortices. When the submerged breakwater does not exist, the vortex disappears completely. In a word, when the porous submerged breakwater exists, the vortex around the submerged breakwater increases, which consumes part of the wave energy and weakens the wave propagation to some extent.

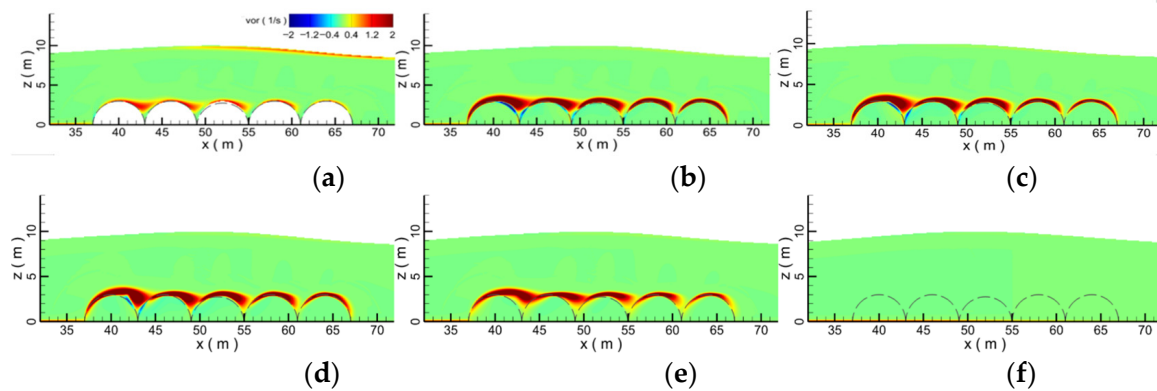


Figure 8. The vorticity contour of the wave peak on the breakwaters under different porosities; (a) por = 0.0; (b) por = 0.2; (c) por = 0.4; (d) por = 0.6; (e) por = 0.8; (f) por = 1.0.

Figure 9 shows the maximum water level and flow velocity monitored at different positions. When the waves reach the submerged breakwater, although the porosity is different, the water level recorded at $x = 10.0$ m is about 9.98 m, and the flow velocity is 2.05 m/s. When the water level is recorded at 20 m, it begins to change. When the porosity is 0.0 and 0.2, the water level is 9.985 m, while when the porosity is 1.0, the minimum water level is 9.95 m. When the monitoring position is at 30 m, the water level obviously rises when there is a submerged breakwater. Because of the existence of the submerged breakwater, the submerged breakwater occupies a part of the water area and the water surface rises. When the monitoring position increases from 40 m to 70 m, the wave energy is dissipated and the water level continues to decrease due to the interference of the submerged breakwater on the water flow. With the increase in porosity, when the porosity is 0.8, the water level reaches a minimum of 9.82 m. When the monitoring position is at

80 m, the wave peak passes through the submerged breakwater, and the water is suddenly released, resulting in a short rise of the water level. Then, the water level gradually drops to a gentle state. When the water passes through the submerged breakwater, the flow velocity also shows an increasing trend, because the submerged breakwater leads to the decrease in the water passing area between the water surface and the submerged breakwater, and the flow velocity increases when the flow flux is constant. When the wave peak passes through the submerged breakwater, the water passing area increases and the flow velocity decreases. In general, when the porosity is 0.8, after the waves pass through the submerged breakwater, the water level decreases significantly, and the wave velocity also decreases.

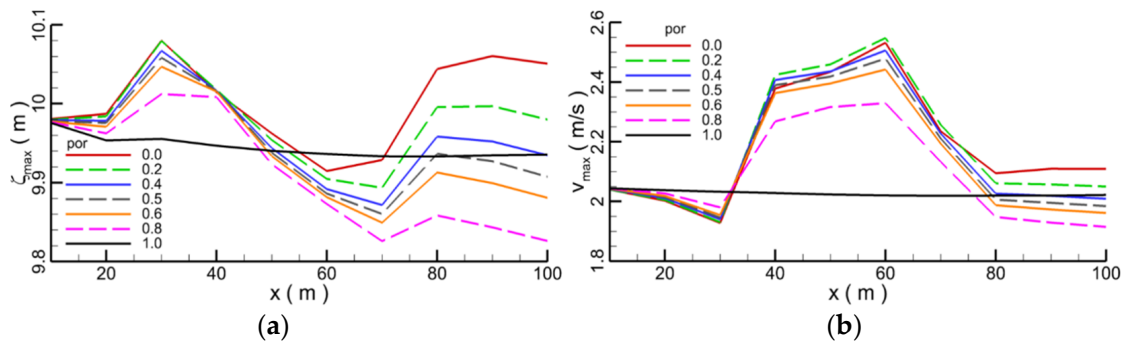


Figure 9. The maximum water level and velocity recorded under different porosities; (a) water level; (b) velocity.

Figure 10 shows the forces of different submerged breakwaters when waves pass through them. With the arrangement of the submerged breakwater from front to back, the force of the submerged breakwater gradually decreases, and the decreasing range gradually decreases, because the front submerged breakwater shields the rear submerged breakwater. With the increase in porosity, the force on the submerged breakwater gradually decreases. When the porosity increases from 0.0 to 0.8, the force on the first submerged bank decreases from 0.66 to 0.13, the force on the second submerged breakwater decreases from 0.67 to 0.14, the force on the third submerged breakwater decreases from 0.65 to 0.13, the force on the fourth submerged breakwater decreases from 0.64 to 0.12, and the force on the fifth submerged bank decreases from 0.62 to 0.11. In a word, submerged breakwaters with different porosity have different effects on wave propagation. When the porosity is 0.8, the force on the submerged breakwaters is the smallest, and the water level and velocity decreases significantly. In order to compare and analyze the force efficiently, the force are normalized by $\rho g v$, i.e., F^* .

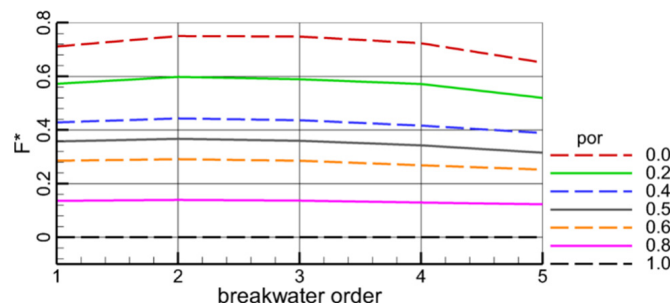


Figure 10. The maximum forces on the breakwaters with the different porosities.

4.2. Effect of the Diameter

This section discusses the influence of submerged breakwaters with different diameters on wave propagation. The porosity of the submerged breakwater is 0.5. According to the survey of the offshore waters of the South China Sea, the average radius of the diving diving dike in the coastal area is about 3 m, so 6 diameters of the submerged breakwater are

selected: 1.5, 2.0, 2.5, 3.0, 3.5, and 4.0 m [36]. Figure 11 shows the velocity contour around the submerged breakwater when the peak reaches the submerged breakwater. When the diameter of the submerged breakwater is 1.5 m, the velocity inside the submerged breakwater is small, and the velocity between the submerged breakwater and the water surface is the largest with the maximum velocity of about 2.1 m/s. With the increase in the diameter, the water area above the submerged breakwater decreases, and the flow velocity increases when the flow flux is constant. When the diameter of the submerged breakwater is 2.5 m, the maximum velocity of the flow field is about 2.5 m/s, and when the diameter of the submerged breakwater is 4.0 m, the maximum velocity of the flow field is 3.0 m/s. In addition, with the increase in the diameter of the submerged breakwater, the profile of the wave gradually becomes flat.

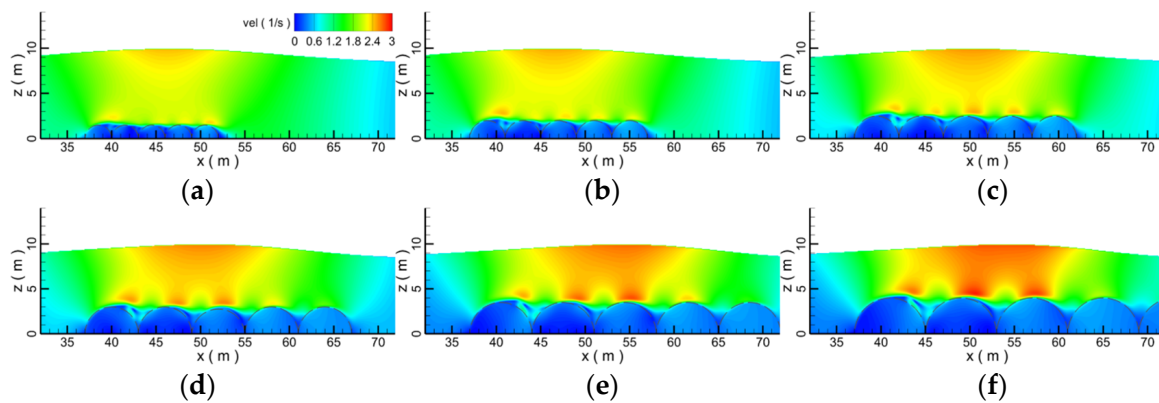


Figure 11. The velocity contour of the wave peak on the breakwaters under different diameters; (a) $D = 1.5$ m; (b) $D = 2.0$ m; (c) $D = 2.5$ m; (d) $D = 3.0$ m; (e) $D = 3.5$ m; (f) $D = 4.0$ m.

Figure 12 shows the vorticity contour around the submerged breakwater when the wave peak is above the submerged breakwater. When the diameter of the submerged breakwater is small, the vortices around the submerged breakwater are connected together to form a flat vortex. With the increase in the diameter of submerged breakwaters, the vortex in the gap between submerged breakwaters is increasing, and the vortex formed by different submerged breakwaters gradually separates, forming a convex circular vortex. When the diameter of the submerged breakwater is 3.5 m, a vortex is attached above each submerged breakwater. A pair of clockwise and counterclockwise vortices can be seen from the first submerged dike. When the diameter of submerged breakwaters is 4.0 m, compared with the vortex formed by submerged breakwaters with other diameters, the vortex reaches the maximum. It shows that the larger the diameter of submerged breakwater is, the stronger the disturbance of convection field is.

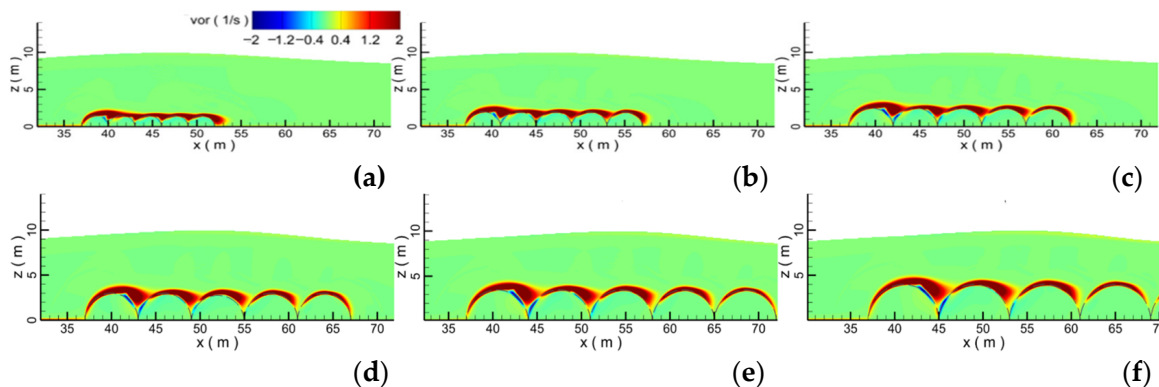


Figure 12. The vorticity contour of the wave peak on the breakwaters under different diameters; (a) $D = 1.5$ m; (b) $D = 2.0$ m; (c) $D = 2.5$ m; (d) $D = 3.0$ m; (e) $D = 3.5$ m; (f) $D = 4.0$ m.

Figure 13 shows the maximum water level and maximum flow velocities recorded at different positions. When the peak reaches the first submerged breakwater, the water area decreases and the water level rises. When the record position is at $x = 30$ m, the maximum water level is 10 m when the diameter of the submerged breakwater is 1.5 m, and the maximum water level is 10.11 m when the diameter of the submerged breakwater is 4.0 m. With the propagation of waves, the wave energy decreases and the maximum water level gradually decreases. When the waves pass through the submerged breakwater, the water level decreases to 9.9 m when the diameter of the submerged breakwater is 1.5 m, and 9.8 m when the diameter of the submerged breakwater is 4.0 m. When the wave reaches the submerged breakwater, the velocity is 2.04 m/s. When the wave peak passes through the submerged breakwater, the flow rate per unit area increases and the velocity increases. When the diameter of the submerged breakwater is 1.5 m, the maximum velocity is 2.2 m/s, and when the diameter of the submerged breakwater is 4.0 m, the maximum velocity is 2.65 m/s. When the peak leaves the submerged breakwater, the velocity of flow decreases rapidly. When the diameter of the submerged breakwater is 4.0 m, the velocity decreases to 1.9 m/s, and when the diameter of the submerged breakwater is 1.5 m, the velocity is 2.0 m/s. When the crest reaches the first diving dike, the water level rises due to the decrease in the area of water crossing, and the flow rate increases under the condition of a certain flow rate. As the waves propagate, the water level decreases, while the speed remains relatively high. The larger the diving dike radius, the greater the water surface rises above the first diving dike, and the water level drops most significantly after passing all the diving dikes. Therefore, the larger the radius of the diving dike, the better the wave absorption effect. In a word, the larger the diameter of submerged breakwater, the more serious the wave water level decreases, and the more severe the fluctuation of velocity, which indicates that the larger the diameter of submerged breakwater, the more significant the attenuation effect on waves.

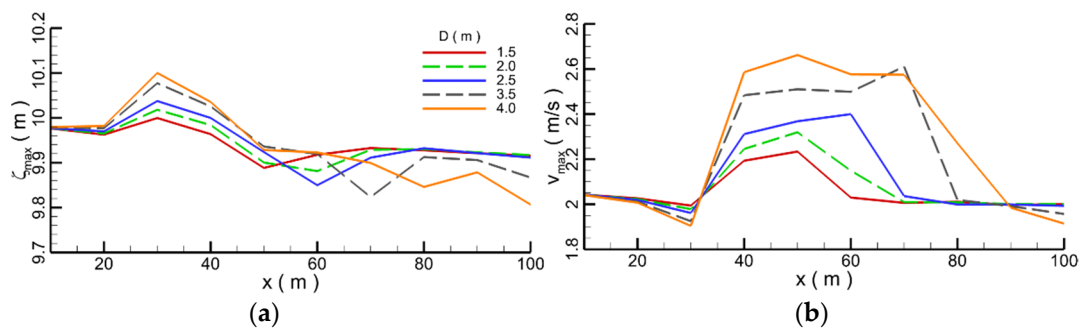


Figure 13. The maximum water level and velocity recorded under different diameters; (a) water level; (b) velocity.

Figure 14 shows the force on submerged breakwaters with different diameters. The front submerged breakwater has a certain protective effect on the rear submerged breakwater. As the submerged breakwater is arranged from front to back, the force on the submerged breakwater with the same diameter gradually decreases. When the diameter of the submerged breakwater is 4.0 m, the force on the submerged breakwater decreases from 0.48 to 0.43. The larger the diameter, the more significant the action of the water body, and the larger the force. When the diameter of the submerged breakwater increases from 1.5 m to 4.0 m, the force on the first submerged breakwater increases from 0.165 to 0.18, and the force on the fifth submerged breakwater increases from 0.16 to 0.43. In general, with the increase in the diameter of the submerged breakwater, the blocking and attenuation effect of the submerged breakwater on waves will increase, and at the same time, the force on the submerged breakwater will also increase. Therefore, the diameter of the submerged breakwater should be selected according to the actual situation, so as to ensure the wave attenuation and maintain the stability of the submerged breakwater. In order to compare and analyze the force efficiently, the force are normalized by $\rho g v$, i.e., F^* .

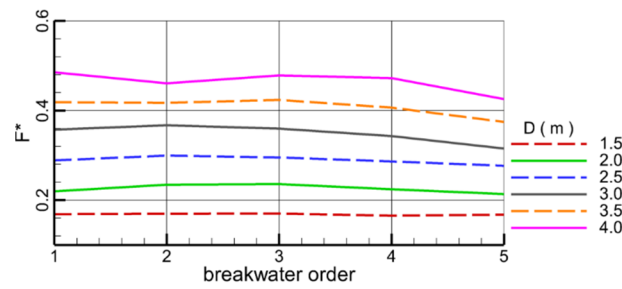


Figure 14. The maximum forces on the breakwaters with different diameters.

4.3. Effect of the Distance

Figure 15 shows the influence of submerged breakwaters with different distances on solitary wave propagation. When solitary waves pass through the submerged breakwater, the velocity above the submerged breakwater is larger, but the velocity in the gap between the submerged breakwaters is smaller. With the increase in the distance, the volume of water in the gap between submerged breakwaters increases, but the flow of water in the gap between submerged breakwaters is weak due to the shelter effect of submerged breakwaters. Although the distance between the submerged breakwaters has a certain influence on wave propagation, the maximum velocity around submerged breakwater in different distances is basically unchanged at about 2.7 m/s. When the distance between submerged breakwaters is 2.4 m, the velocity of water in the gap between submerged breakwaters is basically the same as that in the submerged breakwaters, which indirectly indicates that increasing the distance between submerged breakwaters appropriately is equivalent to increasing the relative length of obstacles, which is conducive to weakening the wave propagation.

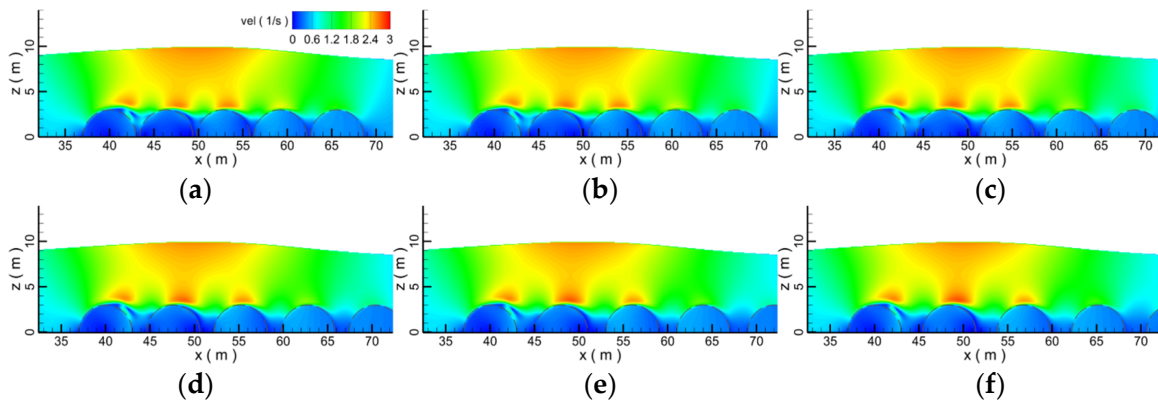


Figure 15. The velocity contour of the wave peak on the breakwaters under different distances; (a) $s = 0.4$ m; (b) $s = 0.8$ m; (c) $s = 1.2$ m; (d) $s = 1.6$ m; (e) $s = 2.0$ m; (f) $s = 2.4$ m.

Figure 16 shows the vorticity contour around the submerged breakwaters with different distances when the wave peak is above a submerged breakwater. The front submerged breakwater has the most significant blocking effect on waves, resulting in the change of water flow. Therefore, the vortex around the front submerged breakwater is the largest. As the submerged breakwaters are arranged backward, the vorticity around the submerged breakwaters gradually decreases. When the distance is 1.6 m, the vortex behind the first submerged breakwater has basically fallen off and filled the gap of the submerged breakwater. With the increase in the distance, the proportion of vortex in the gap decreases, and the vortex basically adheres to the surface of the submerged breakwater, showing the shape of tadpoles. Due to the influence of submerged breakwater seepage, a pair of clockwise and counterclockwise vortices appears on the surface of submerged breakwater. In general, with

the increase in the gap between the submerged breakwaters, the disturbance to the water body is enhanced, and the vortex around the submerged breakwaters is fully developed.

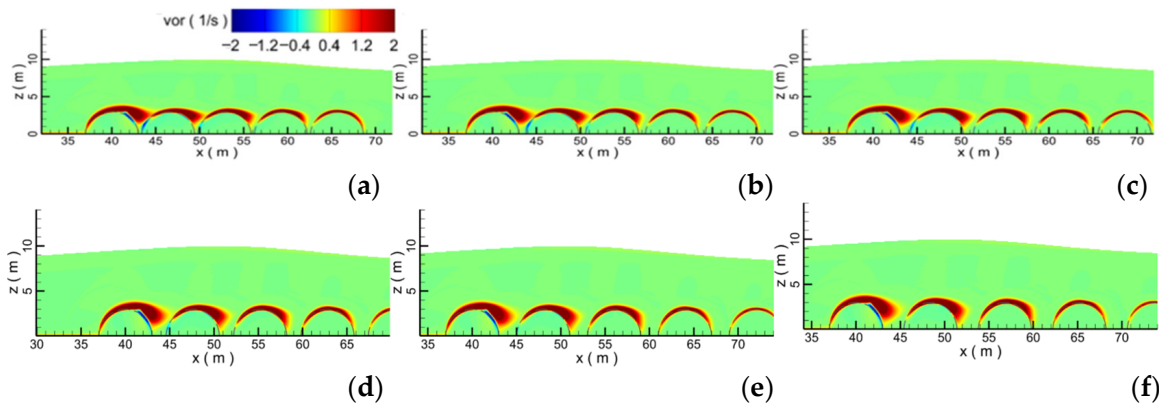


Figure 16. The velocity contour of the wave peak on the breakwaters under different distances; (a) $s = 0.4$ m; (b) $s = 0.8$ m; (c) $s = 1.2$ m; (d) $s = 1.6$ m; (e) $s = 2.0$ m; (f) $s = 2.4$ m.

Figure 17 shows the maximum water level and velocity recorded at different positions when solitary waves pass through submerged breakwaters with different distances. When the recording position is in front of 40 m, due to the existence of the submerged breakwater, the cross-section of the passing water rises, the water level uniformly rises to 10.06 m, and then begins to decline. When the recording position is 70 m, the recorded water level is the lowest. When the clearance is 0.4 m, the water level is 9.82 m, and when the distance is 2.0 m, the water level is 9.86 m. As the monitoring position moves backward and the distance increases, the water level gradually decreases. When the monitoring position is in front of 40 m, the flow rates in different gaps are basically the same. When the monitoring position is 40 m, the flow velocity reaches about 2.4 m/s. With the backward movement of the monitoring position, the monitoring flow velocity gradually decreases, and finally it basically drops to 1.92 m/s. In general, with the increase in the distance, the water level and the flow velocity decrease.

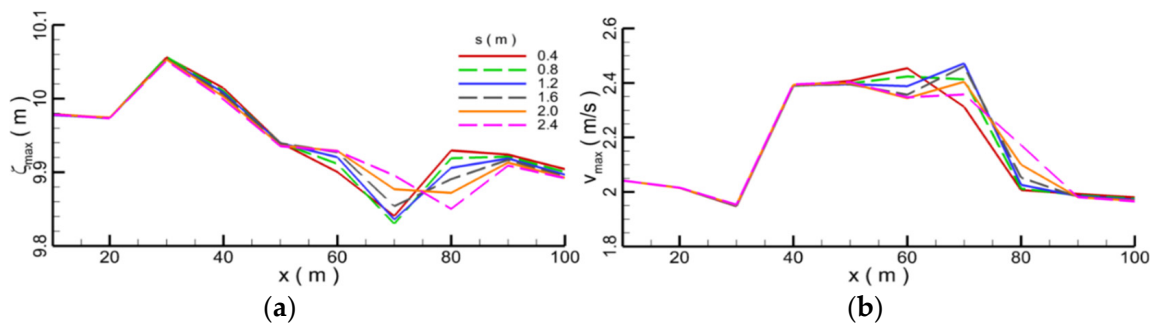


Figure 17. The maximum water level and velocity recorded with different distances; (a) water level; (b) velocity.

Figure 18 shows the maximum forces on different submerged breakwaters under different distances. It can be seen that under the same distance, the force on the second submerged breakwater is greater than that of the first submerged breakwater, because the water flow in the gap in front of the second submerged breakwater is intense, which leads to the larger force on the second submerged breakwater. When the distance is 0 m, the force on the second submerged breakwater is about 0.365, and when the distance is 2.0 m, the force on the second submerged breakwater is about 0.355. As the submerged breakwaters are arranged backward, the force on the submerged breakwaters behind them gradually decreases. When the distance is 0.0 m, the force on the fifth submerged breakwater is 0.32,

and when the distance is 0.4, the force on the fifth submerged breakwater is 0.3. In general, the force on the submerged breakwater in front is greater than that of the submerged breakwater in rear, and with the increase in the gap, the force on the submerged breakwater decreases slightly. In order to compare and analyze the force efficiently, the force are normalized by $\rho g v$, i.e., F^* .

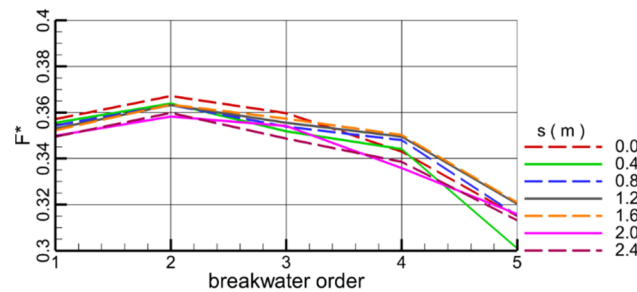


Figure 18. The maximum forces on the breakwaters with different distances.

4.4. Effect of the Wave Height

Due to the different wave heights in the sea, this section mainly discusses the influence of porous submerged breakwater on waves with different wave heights. Seven different wave heights, 1.0, 1.4, 1.8, 2.0, 2.2, 2.6, and 3.0 m, were considered in the study. Figure 19 shows the temporal evolution of the water level and velocity under the different wave heights. With the increase in wave height, the maximum water level and velocity also increase. When the wave height is 1.0 m, the recorded velocity is 0.8 m/s, and when the wave height is 3.0 m, the maximum velocity is 2.9 m/s.

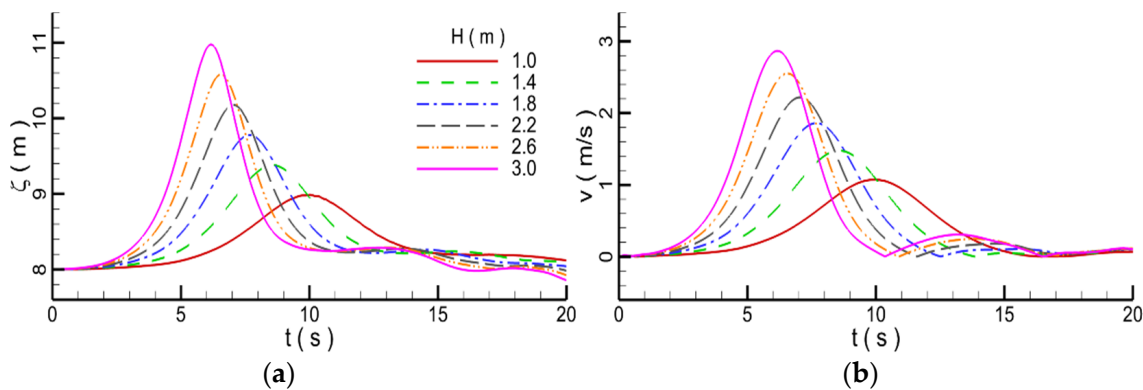


Figure 19. The temporal evolution of the water level and the velocity; (a) the water level; (b) the velocity.

Figure 20 shows the velocity contour around the submerged breakwater with different wave heights. With the increase in wave height, the velocity in the submerged breakwater increases, and the flow velocity between the submerged breakwater and the free water surface also increases. Figure 21 shows the vorticity contour around the submerged breakwater when the wave peaks with different wave heights reach the submerged breakwater. With the increase in wave height, the vorticity around the submerged breakwater increases continuously. When the wave height is 1.0 m, the vortex above the submerged breakwater is long and narrow, and there is no convex hull behind the vortex. When the wave height is 2.2 m, the convex hull formed by the vortex appears behind the submerged breakwater. The higher the wave height, the bigger the vortex behind the submerged breakwater, which indicates that the submerged breakwater has an obvious influence on waves with high wave height.

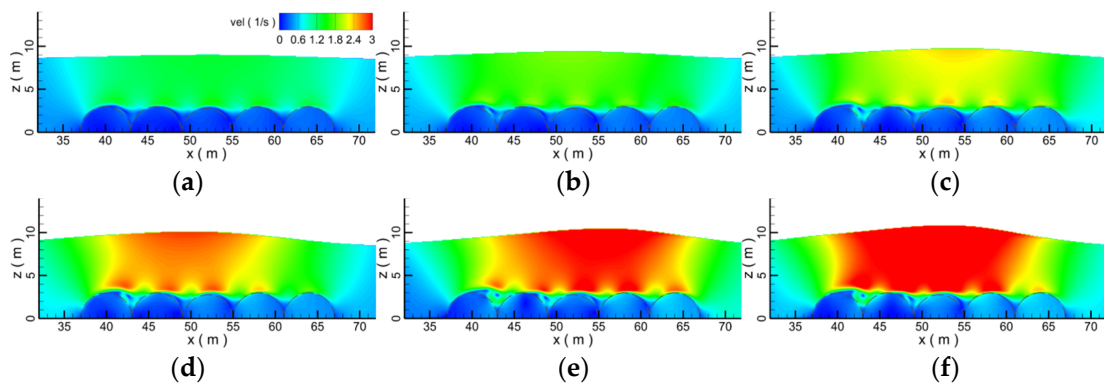


Figure 20. The velocity contour of the wave peak on the breakwaters under different wave heights; (a) $H = 1.0$ m; (b) $H = 1.4$ m; (c) $H = 1.8$ m; (d) $H = 2.2$ m; (e) $H = 2.6$ m; (f) $H = 3.0$ m.

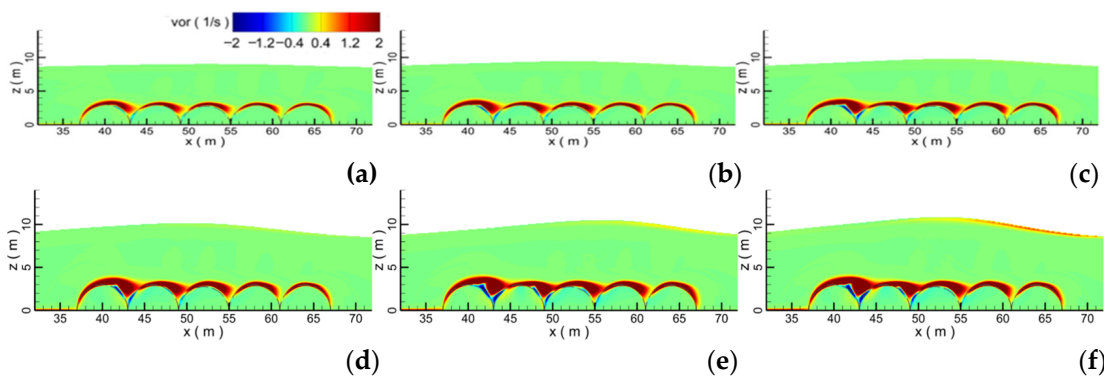


Figure 21. The vorticity contour of the wave peak on the breakwaters under different wave heights; (a) $H = 1.0$ m; (b) $H = 1.4$ m; (c) $H = 1.8$ m; (d) $H = 2.2$ m; (e) $H = 2.6$ m; (f) $H = 3.0$ m.

Figure 22 shows the maximum water levels monitored at different locations. The higher the wave, the more intense the fluctuation of water level. When the wave height is 1.0 m, the maximum water level difference monitored at different positions is 0.2 m, and when the wave height is 3.0 m, the maximum water level difference is 0.5 m, indicating that the higher the wave height, the more serious the influence of submerged breakwater on the waves. With the increase in wave height, the current velocity also increases. When the wave height is 1.0 m, the maximum velocity is 1.3 m/s and the velocity difference is 0.3 m/s. When the wave height is 3.0 m, the maximum velocity is 3.3 m and the velocity difference is 0.6 m/s. In general, with the increase in wave height, the greater the influence of submerged breakwaters on waves, the more energy consumed by wave propagation, and the more obvious the decrease in water level and velocity.

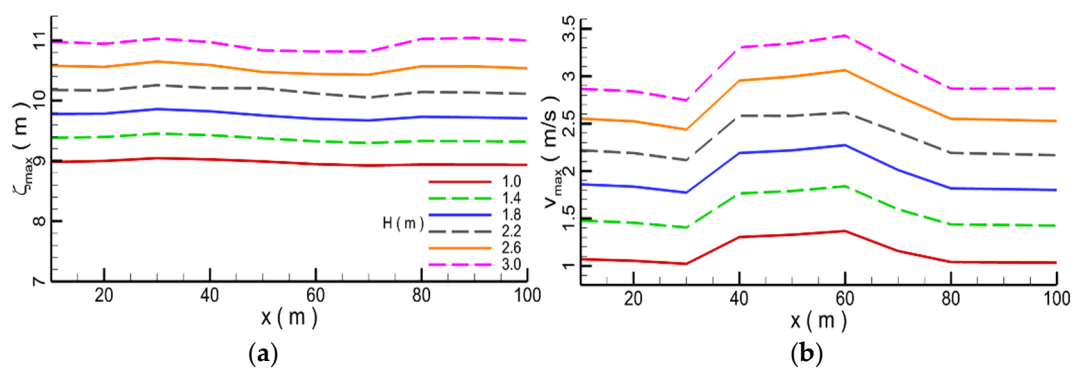


Figure 22. The maximum water level and velocity recorded with different wave heights; (a) water level; (b) velocity.

Figure 23 shows the force on the different submerged breakwaters under solitary waves with different wave heights. The force on the submerged breakwater decreases gradually from the front to the rear, because the front breakwater protects the rear submerged breakwater. When the solitary wave height is 1.0 m, the force from the first to the fifth submerged breakwater decreases from 0.2 to 0.18, and when the solitary wave height is 3.0 m, the force from the first to the fifth submerged breakwater decreases from 0.52 to 0.44. The higher the solitary wave is, the more serious the force on the submerged breakwater is, and the more the force on the submerged breakwater decreases. In general, the higher the wave height, the more obvious the blocking effect of the submerged breakwater on the waves, and the greater the force on the submerged breakwater.

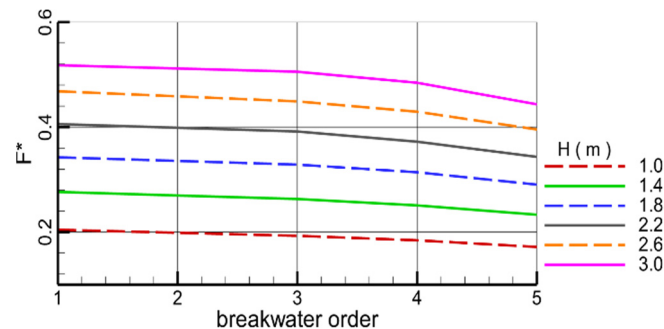


Figure 23. The maximum forces on the breakwaters with different distances.

5. Conclusions

In this paper, the influence of different submerged breakwaters on the propagation of solitary waves with different wave heights is studied by numerical simulation. The main conclusions are as follows:

- (1) Due to the influence of the porous submerged breakwater, at the interface between the water body and the submerged breakwater, the vortex is squashed and presents a strip shape. Submerged breakwaters with different porosities have different interference effects on the flow field, resulting in the change of velocity distribution in the whole flow field, thus affecting the propagation of solitary waves. Submerged breakwaters with different porosities have different effects on wave propagation. When the porosity is 0.8, the force on the submerged breakwaters is the smallest, and the water level and velocity through the submerged breakwaters drop the most seriously.
- (2) With the increase in the diameter of the submerged breakwater, the wave profile gradually becomes flat. When the diameter of submerged breakwaters is 4.0 m, compared with the vortex formed by submerged breakwaters with other diameters, the vortex reaches the maximum. The larger the diameter of submerged breakwater is, the stronger the disturbance of convection field is, the more serious the wave water level decreases, and the more intensive the fluctuation of the velocity, which indicates that the larger the diameter of the submerged breakwater, the more significantly the attenuation effect on the waves. With the increase in the diameter of the submerged breakwater, the blocking and attenuation effect of the submerged breakwater on the waves increases, and at the same time, the force on the submerged breakwater also increases.
- (3) Appropriately increasing the distance between submerged breakwaters is equivalent to increasing the relative length of obstacles, which is conducive to weakening the wave propagation. With the increase in the distance between the submerged breakwaters, the disturbance to the water is enhanced, and the vortex around the submerged breakwaters is fully developed. With the increase in distance, the water level and flow velocity decrease. The force on the submerged breakwater in front is greater than that of the submerged breakwater in rear. With the increase in the distance, the force on the submerged breakwater decreases slightly.
- (4) The higher the wave height, the more serious the wave deformation after passing through the submerged breakwater. The higher the wave height, the bigger the vortex

behind the submerged breakwater, which indicates that the submerged breakwater has serious influence on waves with high wave height. With the increase in wave height, the influence of submerged breakwaters on waves is greater, the energy consumed by wave propagation is greater, and the water level and velocity decrease more obviously. The higher the wave height, the more obvious the blocking effect of the submerged breakwater on the waves, and the greater the force on the submerged breakwater.

- (5) By contrasting with a single breakwater, we obtain the conclusion that the influence of the porous breakwater on wave propagation is more significant than that of the solid breakwater. Additionally, compared with a single breakwater, the porous breakwater has a more significant impact on wave propagation.

Because the submerged breakwater can partially eliminate wave energy and the influence of water waves on the coastline, it has become a common form of breakwater structure in coastal areas. According to the above conclusions, it can be guaranteed to increase the blocking and attenuating effect on the waves under the condition that the submerged breakwater is less stressed. The challenge is that environmental loads can cause damage to the foundation around the submerged breakwater. Therefore, how to reduce the damage is one of the open questions that needs to be faced. In addition, our experiment only studied the isolated wave effects received by one form of breakwater. We will further study the influence of different forms of breakwaters by different waves, such as elliptical waves, sine waves, cosine waves, etc. in the future. It is believed that these research results can be used to better reduce the erosion damage of the coastline by waves.

Author Contributions: Conceptualization, K.Z. and R.J.; methodology, H.Q.; software, Z.C.; validation, Z.S.; investigation, Y.W.; writing—original draft preparation, E.Z. All authors have read and agreed to the published version of the manuscript.

Funding: This research was funded by National Natural Science Foundation of China (Grant No. 52001286; 52101332; 52202427), National Key Research and Development Program of China (Grant No. 2021YFC3101800), Shenzhen Science and Technology Program (Grant No. KCXFZ20211020164015024) and Shenzhen Fundamental Research Program (Grant No. JCYJ20200109110220482).

Institutional Review Board Statement: Not applicable.

Informed Consent Statement: Not applicable.

Data Availability Statement: Not applicable.

Conflicts of Interest: The authors declare no conflict of interest.

Notation List

ρ	fluid density
u	velocity vector in Cartesian coordinate system
t	time
p_r	relative pressure
p	total pressure
g	the acceleration of the gravity
x_r	he reference position coordinate
μ_t	dynamic viscosity
u_p	velocity in the porous medium
γ_p	closure coefficient
ν	kinematic viscosity
d_{50}	median particle diameter of the granular material
KC	Keulegan-Carpenter number
u_r	relative velocity
F	VOF function where when it is filled with water
σ	local coordinate in the relaxation zone
a	wave height of solitary wave
h	initial water depth

References

1. Sun, J.; Ma, Z.; Wang, D.; Dong, S.; Zhou, T. Numerical study of the run-up of a solitary wave after propagation over a saw-tooth-shaped submerged breakwater. *Int. J. Nav. Arch. Ocean Eng.* **2020**, *12*, 283–296. [[CrossRef](#)]
2. Fu, D.; Zhao, X.; Wang, S.; Yan, D. Numerical study on the wave dissipating performance of a submerged heaving plate breakwater. *Ocean Eng.* **2021**, *219*, 108310. [[CrossRef](#)]
3. Zhao, E.; Mu, L.; Hu, Z.; Wang, X.; Sun, J.; Zhang, Z. Physical and Numerical Investigations on Wave Run-Up and Dissipation under Breakwater with Fence Revetment. *J. Mar. Sci. Eng.* **2021**, *9*, 1355. [[CrossRef](#)]
4. Ali, K.K.; El Salam, M.A.A.; Mohamed, E.M.H.; Samet, B.; Kumar, S.; Osman, M.S. Numerical solution for generalized nonlinear fractional integro-differential equations with linear functional arguments using Chebyshev series. *Adv. Differ. Equ.* **2020**, *2020*, 494. [[CrossRef](#)]
5. Osman, M.S.; Rezazadeh, H.; Eslami, M.; Neirameh, A.; Mirzazadeh, M. Analytical study of solitons to Benjamin-Bona-Mahony-Peregrine equation with power law nonlinearity by using three methods. *UPB Sci. Bull. Ser. A Appl. Math. Phys.* **2018**, *80*, 267–278.
6. Akbar, M.A.; Wazwaz, A.-M.; Mahmud, F.; Baleanu, D.; Roy, R.; Barman, H.K.; Mahmoud, W.; Al Sharif, M.A.; Osman, M. Dynamical behavior of solitons of the perturbed nonlinear Schrödinger equation and microtubules through the generalized Kudryashov scheme. *Results Phys.* **2022**, *43*, 106079. [[CrossRef](#)]
7. Han, X.; Dong, S. Interaction of solitary wave with submerged breakwater by smoothed particle hydrodynamics. *Ocean Eng.* **2020**, *216*, 108108. [[CrossRef](#)]
8. Nassiraei, H.; Heidarzadeh, M.; Shafieefar, M. Numerical simulation of long waves (tsunami) forces on caisson breakwaters. *Civ. Eng.* **2016**, *32*, 3–12.
9. Mahmoudof, S.M.; Hajivalie, F. Experimental study of hydraulic response of smooth submerged breakwaters to irregular waves. *Oceanologia* **2021**, *63*, 448–462. [[CrossRef](#)]
10. Zhao, X.; Zhou, Y.; Zong, Y.; Yang, Z.; Luo, M. A CIP-based numerical simulation of wave interaction with a fluid-filled membrane submerged breakwater. *Ocean Eng.* **2022**, *260*, 111819. [[CrossRef](#)]
11. Bautista, E.; Bahena-Jimenez, S.; Quesada-Torres, A.; Méndez, F.; Arcos, E. Interaction between long water waves and two fixed submerged breakwaters of wavy surfaces. *Wave Motion* **2022**, *112*, 102926. [[CrossRef](#)]
12. Chen, Y.-K.; Liu, Y.; Meringolo, D.D.; Hu, J.-M. Study on the hydrodynamics of a twin floating breakwater by using SPH method. *Coast. Eng.* **2023**, *179*, 104230. [[CrossRef](#)]
13. Liang, J.-M.; Chen, Y.-K.; Liu, Y.; Li, A.-J. Hydrodynamic performance of a new box-type breakwater with superstructure: Experimental study and SPH simulation. *Ocean Eng.* **2022**, *266*, 112819. [[CrossRef](#)]
14. Magdalena, I.; Karima, N.; Marcela, I.; Farid, M. Generalization of a three-layer model for wave attenuation in n-block submerged porous breakwater. *Results Eng.* **2022**, *16*, 100428. [[CrossRef](#)]
15. Aristodemo, F.; Filianoti, P. On the stability of submerged rigid breakwaters against solitary waves. *Coast. Eng.* **2022**, *177*, 104196. [[CrossRef](#)]
16. Liang, B.; Wu, G.; Liu, F.; Fan, H.; Li, H. Numerical study of wave transmission over double submerged breakwaters using non-hydrostatic wave model. *Oceanologia* **2015**, *57*, 308–317. [[CrossRef](#)]
17. Lyu, Z.; Liu, Y.; Li, H.; Mori, N. Iterative multipole solution for wave interaction with submerged partially perforated semi-circular breakwater. *Appl. Ocean Res.* **2020**, *97*, 102103. [[CrossRef](#)]
18. Liu, Z.; Wang, Y. Numerical investigations and optimizations of typical submerged box-type floating breakwaters using SPH. *Ocean Eng.* **2020**, *209*, 107475. [[CrossRef](#)]
19. Metallinos, A.S.; Klonaris, G.T.; Memos, C.D.; Dimas, A.A. Hydrodynamic conditions in a submerged porous breakwater. *Ocean Eng.* **2019**, *172*, 712–725. [[CrossRef](#)]
20. Li, X.; Zhang, W. 3D numerical simulation of wave transmission for low-crested and submerged breakwaters. *Coast. Eng.* **2019**, *152*, 103517. [[CrossRef](#)]
21. Xue, S.; Xu, Y.; Xu, G.; Wang, J.; Chen, Q. A novel tri-semicircle shaped submerged breakwater for mitigating wave loads on coastal bridges part I: Efficacy. *Ocean Eng.* **2022**, *245*, 110462. [[CrossRef](#)]
22. Sun, W.; Qu, K.; Kraatz, S.; Deng, B.; Jiang, C. Numerical investigation on performance of submerged porous breakwater to mitigate hydrodynamic loads of coastal bridge deck under solitary wave. *Ocean Eng.* **2020**, *213*, 107660. [[CrossRef](#)]
23. Patil, S.B.; Karmakar, D. Hydrodynamic analysis of floating tunnel with submerged rubble mound breakwater. *Ocean Eng.* **2022**, *264*, 112460. [[CrossRef](#)]
24. He, Y.; Ji, W.; Han, B.; Yan, L.; Han, X. Influence of submerged annular rippled breakwater on hydrodynamic performance of column floating pier. *Ocean Eng.* **2022**, *247*, 110756. [[CrossRef](#)]
25. Zhao, E.; Dong, Y.; Tang, Y.; Xia, X. Performance of submerged semi-circular breakwater under solitary wave in consideration of porous media. *Ocean Eng.* **2021**, *223*, 108573. [[CrossRef](#)]
26. Guo, Y.; Mohapatra, S.; Soares, C.G. Submerged breakwater of a flexible porous membrane with a vertical flexible porous wall over variable bottom topography. *Ocean Eng.* **2021**, *243*, 109989. [[CrossRef](#)]
27. Koley, S.; Vijay, K.; Nishad, C.; Sundaravadivelu, R. Performance of a submerged flexible membrane and a breakwater in the presence of a seawall. *Appl. Ocean Res.* **2022**, *124*, 103203. [[CrossRef](#)]

28. Koraim, A.; Heikal, E.; Zaid, A.A. Hydrodynamic characteristics of porous seawall protected by submerged breakwater. *Appl. Ocean Res.* **2014**, *46*, 1–14. [[CrossRef](#)]
29. Jensen, B.; Jacobsen, N.G.; Christensen, E.D. Investigations on the porous media equations and resistance coefficients for coastal structures. *Coast. Eng.* **2014**, *84*, 56–72. [[CrossRef](#)]
30. van Gent, M.R.A. Porous Flow through Rubble-Mound Material. *J. Waterw. Port Coast. Ocean. Eng.* **1995**, *121*, 176–181. [[CrossRef](#)]
31. Zhao, E.; Qu, K.; Mu, L. Numerical study of morphological response of the sandy bed after tsunami-like wave overtopping an impermeable seawall. *Ocean Eng.* **2019**, *186*, 106076. [[CrossRef](#)]
32. Zhao, E.; Shi, B.; Qu, K.; Dong, W.; Zhang, J. Experimental and Numerical Investigation of Local Scour around Submarine Piggyback Pipeline under Steady Current. *J. Ocean Univ. China* **2018**, *17*, 244–256. [[CrossRef](#)]
33. Zhao, E.; Dong, Y.; Tang, Y.; Cui, L. Numerical study on hydrodynamic load and vibration of pipeline exerted by submarine debris flow. *Ocean Eng.* **2021**, *239*, 109754. [[CrossRef](#)]
34. Zhao, E.; Dong, Y.; Tang, Y.; Sun, J. Numerical investigation of hydrodynamic characteristics and local scour mechanism around submarine pipelines under joint effect of solitary waves and currents. *Ocean Eng.* **2021**, *222*, 108553. [[CrossRef](#)]
35. Wu, Y.-T.; Hsiao, S.-C. Propagation of solitary waves over a submerged permeable breakwater. *Coast. Eng.* **2013**, *81*, 1–18. [[CrossRef](#)]
36. Ye, J.H.; He, K.P.; Shan, J.P. Experimental Study on Stability of Revetment Breakwater Built on Reclaimed Coral Reef Islands in South China Sea under Extreme Wave Impact. *Blasting* **2019**, *36*, 11. [[CrossRef](#)]

Disclaimer/Publisher’s Note: The statements, opinions and data contained in all publications are solely those of the individual author(s) and contributor(s) and not of MDPI and/or the editor(s). MDPI and/or the editor(s) disclaim responsibility for any injury to people or property resulting from any ideas, methods, instructions or products referred to in the content.